Analysis of the track system in bumpy unstructured hard road environment by vibration test

Mutong Li[1*], Junlue Li[1], Lin He[1], Jie He[2], Lian Hu[2], Chengxu Lyu[3]

(1. *Key Laboratory of Modern Agricultural Intelligent Equipment in South China, Ministry of Agriculture and Rural Affairs, China / Guangdong Institute of Modern Agricultural Equipment, Guangzhou 510630, China*;
2. *College of Engineering, South China Agricultural University, Guangzhou 510642, China*;
3. *Chinese Academy of Agricultural Mechanization Sciences, Beijing 100083, China*)

Abstract: The complex terrain environment in the hilly land directly affects the operational reliability of agricultural robots. In order to study the impact of road irregularity on walking chassis vibration, the 3CYLZ-750 remote-controlled weeding machine which is applied to orchards was taken as the object of study, and the rear roller was selected as the object of observation to reveal the rules under which the vibration of the track chassis changes as there is a sudden change in road surface elevation. A column-type test-to-pass method based on unit excitation was proposed in this study. The excitation behavior and action process were analyzed by category. A critical acceleration prediction model was built and verified by virtual simulation and hard road surface excitation testing. The results showed that at the forward velocity of 0-2.5 km/h and exciter height of 20-100 mm, the vertical vibration acceleration of the target roller was significantly affected by Track Contact Point Centrifugal Acceleration (TCPCA). As TCPCA increased, the change rate of vertical vibration acceleration decreased, reaching a minimum of [−13.8, 28.8]; as TCPCA decreased, the vertical vibration acceleration tended to increase positively at a maximum variation range of [−13.3, 42.2]. The measured and simulated macroscopic change rules were consistent with the theoretical analysis, further verifying the correctness of variable extraction, and providing a research basis for the accurate modification and improvement of the model. The research conclusions can lay a theoretical foundation for analyzing the walking reliability of the track chassis, and provide a design basis and technical support for the development of a tracked agricultural robot chassis for the hilly land in the future.

Keywords: track system, unstructured road, vibration test, simulation analysis, hilly land, agricultural robot
DOI: 10.25165/j.ijabe.20221504.7249

Citation: Li M T, Li J L, He L, He J, Hu L, Lyu C X. Analysis of the track system in bumpy unstructured hard road environment by vibration test. Int J Agric & Biol Eng, 2022; 15(4): 163–171.

1 Introduction

With the year-by-year standardization and technological development of modern agriculture in recent years, the key technologies related to agricultural robots have become a hot topic for contemporary engineers. Especially, when it comes to the research on applying many flexible track robots in complex terrain environments such as hilly land, researchers and some scholars have conducted in-depth research on the mechanism of robot-soil interaction and robot behaviors, such as obstacles and ditch crossing, using numerical simulation[1]. However, during the process of intelligent improvement and upgrading of agricultural machinery and equipment for complex terrain environments, problems of body nonlinearity, such as violent vibration and impact, are often caused by many factors including the change of body gravity, road irregularity, soft soil subsidence, and soil sliding. This type of harmful vibration directly affects the reliability of the actuator mounted on the agricultural robot, and also has a negative impact on the working performance of the core intelligent components[2,3]. Therefore, a clear understanding of the vibration generation mechanism and transmission law of the track chassis system in the walking process is of important theoretical guiding significance for the design and development of agricultural robots and provides a necessary reference for the development of key components.

There is quite complicated interactive vibration between the track chassis and the soil surface. According to the current research findings, the walking chassis mainly involves behaviors including soil subsidence[4-6], track envelope deformation[7,8], and immediate movement of roller carrier[9], etc. At present, there are many research directions. Most scholars define the soil model based on the pressure-subsidence relationship and contact force proposed by Beker[10-12]. They also build a model for the rigid track and analyze the soil surface excitation response using dynamical analysis software[13-15]. This method cannot be well applied to the calculation of rubber tracks, because it is mostly used for articulated track treads for which external pattern characteristics are ignored. Besides, the deformation of the soil surface is mostly simulated finite element method (FEM). Despite a rise in the simulation velocity, the simulation results are greatly different from the actual value, and therefore cannot be used as an effective

Received date: 2021-12-07 **Accepted date:** 2022-04-15
Biographies: Junlue Li, MBA, research interests: planning of agricultural machinery and equipment in South China, Email: lijunlue@188.com; **Lin He**, MBA, research interests: design of agricultural machinery in hilly and mountainous areas, Email: 75318013@qq.com; **Jie He**, PhD, research interests: path planning and navigation of agricultural machinery, Email: hooget@scau.edu.cn; **Lian Hu**, PhD, research interests: path planning and navigation of agricultural machinery, Email: lianhu@scau.edu.cn; **Chengxu Lyu**, PhD, research interests: target recognition and image processing, Email: lvchengxu@caams.org.cn.
***Corresponding author: Mutong Li**, PhD, Senior Engineer, research interests: reliability technology of agricultural machinery in Hilly Area. Guangdong Institute of Modern Agricultural Equipment, Guangzhou, China. Tel: +86-18312222400, Email: 236280045@qq.com.

reference for research. Currently, there are some methods for soft road surface modeling proposed in the available literature. Nishiyama et al.[16,17] argued that an FE-DEM continuous swap model could be built to shorten the simulation time by 23% or so, but this method remained limited to calculations in 2D space. There are still very few existing studies on the walking vibration of the track chassis system. For example, Nakata et al.[18] analyzed the vibration characteristics of tracked agricultural vehicles on different roads under the ISO standards. They also analyzed the effects of two kinds of rubber tracks (with an iron core and without an iron core) on vibration damping and the impact of vibration on the human body; Sundaram et al.[19] performed rigid-flexible classified modeling for the suspension unit in the track roller train, and compared the dynamic characteristics, finding that FEM could be used to analyze the effect of the dynamic vibration of the track roller arm; Xu et al.[20] took the seats in the tracked combine as objects of observation and conducted an experimental study on the vibration characteristics, finding that the suspension system played an important role in vibration transmission attenuation. In summary, there remains a lack of a proper method for agricultural track system modeling, and there are still very few analyses or experimental studies on the excitation vibration of the track on roads. This is also a technical bottleneck for the future development of a tracked agricultural robot applied to complex terrain environments.

A column-type test-to-pass method based on unit excitation was proposed in this study on the basis of the above research foundation and background. Then, by reference to the vibration transmission and evaluation methods from the road surface of the moving wheel train to the chassis as a whole as well as the vibration test measurement methods and other standards[21-23], with the track chassis of the 3CYLZ-750[24] remote-controlled weeding machine as the object of study, the vertical excitation action of the walking speed and cylindrical diameter (exciter elevation, i.e., height) on each roller, as well as the change rule and range of vibration acceleration, was studied at different levels. The conclusion can provide reference and technical support for the design and development of tracked agricultural robots applied to complex terrain environments.

2 Analysis of basic principle

2.1 Condition setting

As the track chassis moves forward, the exciters at different heights on the road surface act differently on the track. Given low exciter height, the trapezoidal sloping structure of the patterned outside surface of the track will push most of the exciter into the sunken area in the contact process, then achieving an envelope effect through structural gaps. At this time, the inside of the track can be considered non-deformed, while the chassis roller train does not suffer from obvious vertical displacement. This process is defined as a non-deformation envelope in this study, as shown in Figure 1a; given great exciter height, the gap enveloping ability of the patterned outside surface of the track will fail, and the track between the rollers will suffer from flexural deformation to some extent under the action of the exciter. In this process, the chassis roller train suffers from vertical displacement to some extent under the action of the exciter. This process is defined as a deformation envelope in this study, as shown in Figure 1b.

In the present study, the road surface structure envelope and vibration characteristics involved in the longitudinal walking process of the track system were mainly analyzed, while problems concerning large displacements, such as obstacle crossing, slope climbing, and ditch crossing, were not discussed. Neither was a detailed study conducted on other problems such as the probabilistic envelopes of track patterns and granules. Therefore, for the deformation and its process, only some road environments meeting the geometric trafficability condition were selected, and by reference to the obstacle-crossing conditions for track vehicles proposed by Kuhner[25] and Zhang[26], cylindrical steel was chosen as external exciters, which were mounted on the surface of the road on which the tested machine would move forward. The range of exciter height was set as follows:

$$H_R \in [h_\delta, h_{sw}] \quad (1)$$

where, H_R represents the height of the exciters, and also the cylindrical diameter of the exciters in this study, mm; h_δ represents the height or thickness of track patterns, mm; h_{sw} represents the vertical height between the center of the rollers and the road surface, mm.

The 3CYLZ-750 remote-controlled weeding machine was taken as the object of study in this study. Its center of mass is located between the front roller and the middle roller. When the track chassis moves forward at a constant speed, track walking at full-ground-contact size is regarded as the initial state, as shown in Figure 2.

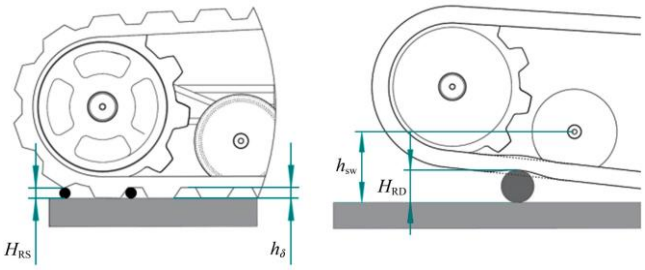

a. Non-deformation envelope b. Deformation envelope

Note: H_{RS} represents the height of the exciter that will not cause the deformation of the track, mm; H_{RD} represents the height of the exciter that will cause the deformation of the track, and also the cylindrical diameter of the exciters in this study, mm; h_δ represents the height or thickness of track patterns, mm; h_{sw} represents the vertical height between the center of the rollers and the road surface, mm.

Figure 1 Classification of the envelope processes of exciters at different heights

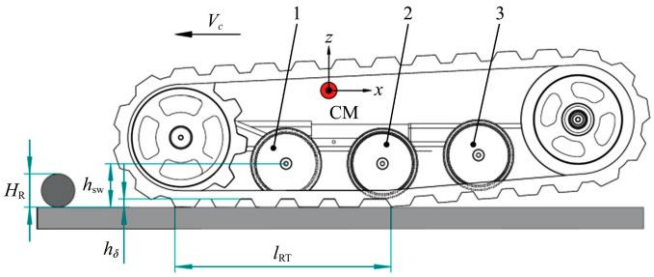

1. Front roller 2. Middle roller 3. Rear roller

Note: CM represents the chassis centroid; V_c represents the moving speed of the chassis in the forward direction, km/h; H_R represents the height of the exciters, and also the cylindrical diameter of the exciters in this study, mm; l_{RT} represents the length of the ground-contact area when the track is in the default driving state, mm; The z-axis direction is the vertical direction, while the x-axis direction is the moving direction of the track chassis. In this study, h_{sw} was set to 102 mm while h_δ was set to 15 mm.

Figure 2 Diagrammatic sketch of excitation model for track chassis walking on a hard road surface

2.2 Motion decomposition

The vibration effect of the track roller train is mainly reflected in the vertical impact force, vibration energy, and vibration gap.

Moreover, considering the diversified combination of the driving roller and guide roller in terms of form and structure, the roller, which touches the ground frequently, was selected as an object of analysis in the present study to further analyze the change rule of its vertical acceleration component. For the change in the vertical acceleration of the target roller, it is mainly affected by factors including the forward velocity, the pitch angle of the chassis, the exciter height, the coefficient of friction between the track and the exciter, and the location of the center of mass of the machine. Therefore, the action of the track chassis walking through the exciter needs to be decomposed for the sake of accurate calculation and analysis.

First, the entire track is regarded as a non-deformable material. As shown in Figure 3, the process in which the track chassis walks through the exciters set on the road surface is divided into five parts, including (I) stable state, (II) forward state, (III) critical state, (IV) downward state, and (V) disengaged state.

It should be noted that in (II) and (IV), the ground provides a certain supporting force for the chassis, getting it into an almost stable state of motion. In (III), neither end of the chassis touches the ground, suggesting that the chassis is in an unstable state of motion. Therefore, the motion characteristics in (III), the critical state, are deeply studied in this study. Besides, it should be specially noted, "When the chassis climbs over the highest point in the vertical direction, the vertical velocity component is zero (at the moment when the rear end of the track is disengaging from the ground). This instantaneous position is the starting point of (III), the critical state, and at the moment when the front end of the track touches the ground, this instantaneous position is the ending point of (III), the critical state.

Therefore, an important basis and be laid for subsistent subsequent dynamic analysis and mathematical modeling by decomposing the above-mentioned action of the track chassis walking through the exciters and defining it piecewise.

2.3 Modeling

There is the constant tangent velocity at the point of tangency where the track touches the surface of the exciter. For the convenience of calculation, it is defined in this study that there always exists track contact point centrifugal acceleration (TCPCA) at the point of tangency P' between the lower surface of the track and the surface of the exciter. Its value, which is set in varying proportions under initial working conditions, is equal to the ratio of the square of the tangent velocity of the track to the radius of the exciter.

$$a_C = \frac{2V_{P'}^2}{H_R} \tag{2}$$

where, a_c represents the centrifugal acceleration at point p', m/s^2; $V_{p'}$ represents the instantaneous tangent velocity in the critical state, m/s.

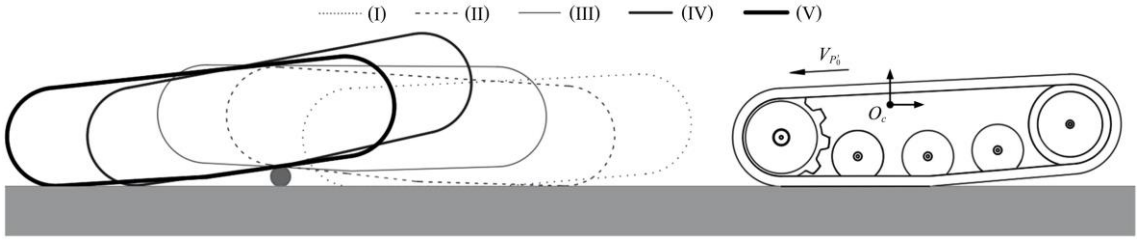

Note: (I) stable state; (II) forward state; (III) critical state; (IV) downward state; (V) disengaged state. V_P represents the instantaneous tangent velocity in the critical state, m/s; *Oc* represents the centroid of the chassis, the same as cm in the above figure.

Figure 3 Schematic diagram of action decomposition at the stage of track chassis excitation

According to Figure 3 and Figure 4, in (III), the critical state, the point of tangency P moves along the outer circular locus of the exciter to point P' over time. Suppose the track remains in contact with the surface of the exciter all the time and there is no relative slip. So, point P' will move at variable speed in a circle around the center O_o of the exciter, and the resultant external force borne by it comes primarily from the friction force between the track and the exciter surface and its gravity component.

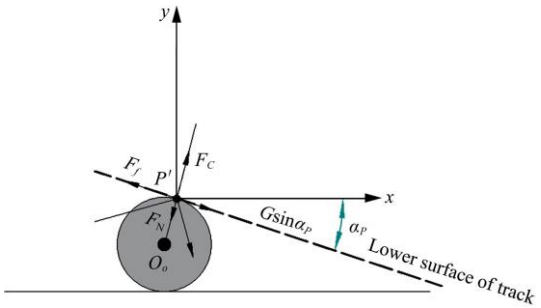

Note: F_C represent the instantaneous centrifugal force at the contact tangent point between the track and the exciter, N; F_N represents the normal support force of the contact point between the surface of the exciter and the track, N; F_f represents the friction between the track and the surface of the exciter, N; $G\sin\alpha_P$ represent the dynamic component of gravity in the tangent direction between the track and the exciter, N; α_P represent the chassis pitch angle, rad .

Figure 4 Schematic diagram of force at the point of tangency at the starting point of critical state

Therefore, in order to accurately analyze the motion characteristics of the chassis in the vertical direction, a rectangular coordinate system was established with P' as the origin. According to the analysis results, the tangential acceleration and normal acceleration at P' are as follows:

$$\begin{cases} a_{\tau P'} = \mu a_{nP'} + g\sin\alpha_P \\ a_{nP'} = g\cos\alpha_P - a_C \end{cases} \tag{3}$$

where, $a_{nP'}$ represents the normal acceleration of tangent point p', m/s^2; a_c represents the centrifugal acceleration at point p', m/s^2; α_P represents the angle between p' tangent and horizontal plane, is a dynamic quantity, rad; $a_{\tau p'}$ represents the tangential acceleration of tangent point p', m/s^2; μ represents the coefficient of friction between the track and the exciter. Considering the pattern structure of the track and its flexible grip characteristics, the coefficient of static friction is selected for calculation in this study, μ=0.9; g represents the acceleration of gravity, g=9.8 m/s^2.

In the orthogonal vertical direction, there is

$$a_{YP'}=a_{\tau P'}\sin\alpha_P \tag{4}$$

where, $a_{YP'}$ represents acceleration of p' point in Y-axis direction of the orthogonal coordinate system, m/s^2.

As shown in Figure 5, the relationship between the center of mass, the driving roller center, and the rear roller center in terms of vertical acceleration can be further calculated.

2.4 Variable analysis

The pitch angle α_P of the chassis will change from a negative

value to a positive value in the process of obstacle crossing, in which the static friction of track patterns serves as the main driving force. Therefore, in order to ensure that "horizontal projectile hovering" does not occur when the chassis moves through the top of the exciter, its instantaneous normal acceleration $a_{nP}>0$, so the centrifugal acceleration at P' can be known as $a_C=\frac{2V_{P'}^2}{H_R}<g$, with the variable value range further determined.

Because the rear roller, the object of this study, was located at the far center of mass, there exists a maximum vertical displacement in the critical state. So, the rear roller was selected as the object of observation for easy measurements in the test. Considering the rigid track mentioned in the above theoretical analysis, the vertical acceleration a_{Ysw} of the target roller is equal to the vertical acceleration $a_{YP'}$ at the point of tangency in the same inertial system. On the basis of the above constraint conditions, a function can be established for the vertical acceleration $a_{YP'}$ at the point of tangency with respect to α_P and a_C by combining Equation (3) with Equation (4), and then imported into the software Origin to generate corresponding response surface. As shown in Figure 6, the change rule of the vertical acceleration of the target roller can be determined.

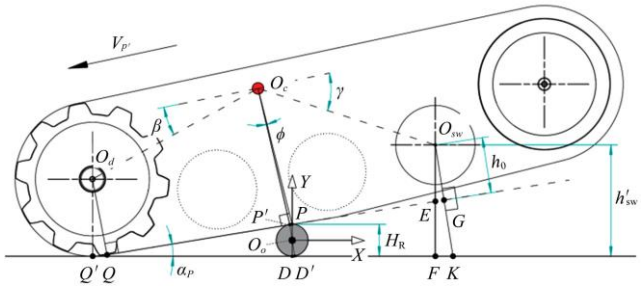

Note: O_d represents the center point of the driving wheel; O_{sw} represents the center point of the supporting roller; O_o represents the center point of the excitation body; Q' is the point of intersection between the driving roller center O_d and the perpendicular line on the lower end face of the track. It is also called the ground-contact point in this study. h_0 represents the ground clearance of the rear roller in the stable state (I); h'_{sw} represents the ground clearance of the supporting roller at the moment of termination in the critical state (III); β represents the angle between the center-of-mass coordinate plane and O_cO_d, set to $10\pi/9$; γ represents the angle between the center-of-mass coordinate plane and O_cO_{sw}, set to $-3\pi/20$; $l_{OcP'}$ represents the line between the center of mass and the point of tangency, $\varphi=\alpha+\pi/2$ in the critical state (III).

Figure 5 Ending point in the critical state (III) and key parameters

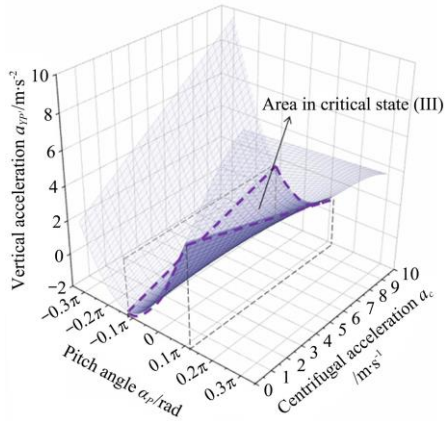

Note: The purple thick dash line in the figure delineates an effective area for the critical state (III), while the corresponding two planes delineated by black dash lines are $\alpha_{Pmin}=-0.12\pi$ and $\alpha_{Pmax}=0.11\pi$, respectively. The transparent surface area is inefficient, and not selected for calculations in this study.

Figure 6 Effects of centrifugal acceleration at different levels and pitch angle tangential acceleration on acceleration

The centrifugal acceleration a_c at the point of contact set in this study was mainly determined according to the selected working parameters. The height H_R of the exciter was set to 0.015-0.102 m in this study. According to the results of the analysis of the above variables, $V_{P'\max}<\sqrt{\frac{gH_R}{2}}$. Also, the maximum forward velocity $V_{P(\max)}$ corresponding to the height H_R of the exciter at different levels is obtained. Further, the relationship between the values of $a_c/V_{P'}$ and H_R was revealed, as shown in Figure 6 and Figure 7.

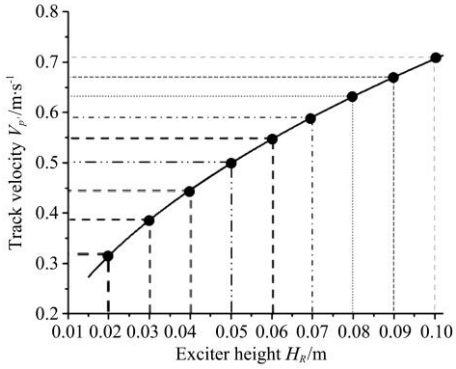

Note: Exciter height $H_R\in[h_\delta, h_{sw}]$, to be specific, h_δ is set to 15 mm, and h_{sw} is set to 102 mm in the model of this study.

Figure 7 Maximum track velocity corresponding to different levels of the height of the exciter

According to Figure 6 and Figure 8, when the pitch angle is negative, TCPCA is positively correlated with the vertical acceleration, and the acceleration changes greatly; when the pitch angle is positive, TCPCA is negatively correlated with the vertical acceleration, and the change amplitude decreases with the increase of the pitch angle. In summary, as the pitch angle gradually increases, the vertical acceleration a decreasing-increasing-decreasing trend.

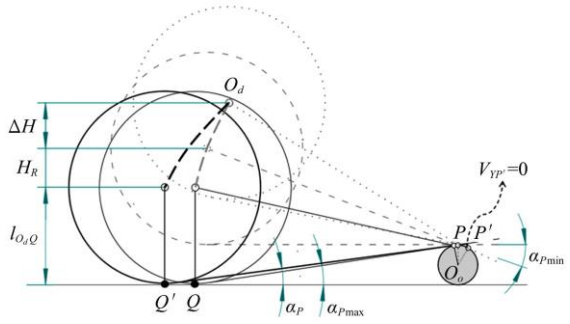

Note: l_{OdQ} represent the vertical distance between driving wheel center and grounding point, mm; H_R represents the exciter height, mm; ΔH represents the vertical change of wheel center when the driving wheel slides from the highest point to the time when the touched-ground plane is parallel to the horizontal plane, mm; $V_{YP'}$ represent the linear velocity of the dynamic tangent point between the track and the surface of the exciter, m/s; α_P represents the chassis pitch angle, rad; α_{Pmin} and α_{Pmax} represent the minimum and maximum values of pitch angle, rad.

Figure 8 Schematic sketch of quasi-horizontal projectile motion of the track in the ground-contact area

According to the actual analysis, under the condition of centrifugal acceleration at different points of contact, $\alpha_P\in(\alpha_{Pmin}, \alpha_{Pmax})$ for the chassis in the critical state (III). When $V_{YP'}=0$, the pitch angle of the chassis reaches its minimum, and its variation range $\alpha_{Pmin}\in(-0.12\pi, 0)$; when the front end of the track touches the ground, the pitch angle of the chassis reaches its maximum α_{Pmax}. As shown in Figure 8, the virtual displacement

method is adopted to specify the track velocity $V_{P'}$=0 when $V_{YP'}$=0. At this time, the chassis is turned forward around the center O_o of the exciter until it touches the ground, so,

$$\alpha_{P\max} \approx \arctan(\frac{H_R}{l_{QP}}) \geq \alpha_P \tag{5}$$

According to the known parameters adopted in the model of this study: l_{OcOd}=292 mm, l_{QP}=277 mm, l_{OcP}=239 mm, $l_{OcP'}$=236 mm, and l_{OcOsw}=281 mm, the pitch angle of the chassis can reach its maximum $\alpha_{P\max}\in(0.02\pi, 0.11\pi)$. According to the above analysis, the effective area in Figure 6 is further delineated.

2.5 Model modification

In practice, if the track chassis is powered by the fuel engine, test results of vibration acceleration should include the self-excited vibration of the engine; also, there exists a deformation envelope and buffer effect in the process in which the rubber track passes through the exciter, so,

$$a'_{Ysw} = \xi \cdot a_{YP'} + a_{YEsw} \tag{6}$$

where, a'_{Ysw} represents the correction of the vertical acceleration of the target roller, m/s^2; ξ represents the vertical buffer coefficient at the point of tangency between the track and the exciter. Its value range from 0 to 1 and is temporarily set to 1 in this study. Its value depends on multiple factors such as the pre-tightening force of the track. The relevant study will be published later, and won't be described in detail in this study. a_{YEsw} represents the vertical acceleration at the rear roller center when the engine is idling. At the rated speed of 3600 r/min, the specific value should be set according to the effective convergence value of its working state measured by a test, and finally used as a constant term for calculation[27,28].

3 Test design

3.1 Object of test

The 3CYLZ-750 remote-controlled weeding machine[24], which is applied to orchards, made by the Guangdong Hongke Agricultural Machinery R&D Co., Ltd., was selected as an experimental prototype. The machine consists of a tracked chassis, a power unit, a hydraulic system, a weeding component, a control box, and a protective housing (Figure 9).

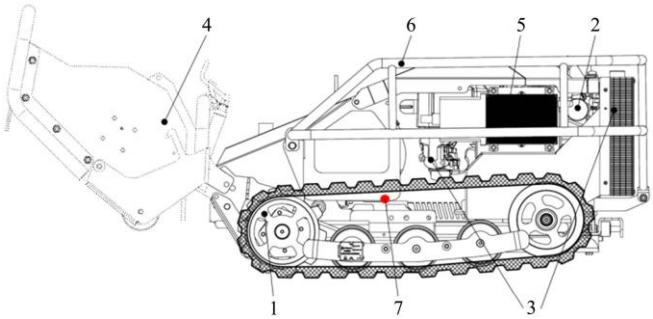

1. Track chassis 2. Power unit 3. Hydraulic system 4. Weeding unit
5. Control box 6. Protective housing 7. Center of mass of the machine

Figure 9 Structural schematic diagram of 3CYLZ-750 remote-controlled weeding machine

The track system of this experimental prototype consists primarily of a driving roller, rollers, and a guide roller that matches with the tensioning rod, which is commonly applied to most agricultural robots. With an iron core glued to it through a fiber thread and high-density rubber, the track, which has good flexibility and elasticity, has excellent grip performance and envelope deformability. The main parameters of the whole machine are listed in Table 1.

3.2 Test schemes

TCPCA was taken as the test factor in this study, its value is equal to the ratio of the square of forward velocity to the radius of the exciter. The maximum vertical acceleration of the rear roller that is far away from the center of mass was selected as the evaluation index. The height of the exciter was set to 0.02-0.10 m. According to the above conclusion, the track velocity was set as follows in this test:

$$\sqrt{\frac{gH_{R(i-1)}}{2}} < V_c < \sqrt{\frac{gH_{R(i)}}{2}} \tag{7}$$

where, i represents the horizontal number of the exciter height, $i\in[1,9]$.

Table 1 Main parameters of 3CYLZ-750 remote-controlled weeding machine

Basic parameters	Value
Overall dimension/mm×mm×mm	1877×865×600
Machine mass/kg	340
Engine power/kW	9.5
Rated displacement of hydraulic pump/mL r^{-1}	6
Hydraulic motor specification/(N m/(r min^{-1}))	240/(0-480)
Power supply/V	12
Moving velocity/km h^{-1}	0-6 (0-1.67 m/s)
Track size (Width × Pitch × Number of Pitches) /mm×mm×mm	150×72×30
Pattern height/mm	33.5
Gauge/mm	645
Grounding length/mm	432
Remote control range/m	0-150

Because there was an obvious interaction between the two factors in this study and limits for the value range, nine groups of different test schemes were designed according to the maximum forward velocity limits corresponding to the exciter height at different levels. Table 2 lists the working conditions for the simulation and road surface excitation test.

Table 2 Test factor value between forward velocity and exciter height matching table

Test group	Factors			
	Maximum forward velocity $V_{c(\max)}$/m s^{-1}	Test value of forward velocity $V_{c(\text{test})}$/m s^{-1}	Exciter height H_R/mm	TCPCA a_c/m s^{-2}
1	0.32	0.30	20	4.50
2	0.39	0.35	30	4.08
3	0.45	0.40	40	4.00
4	0.50	0.45	50	4.05
5	0.55	0.50	60	4.16
6	0.59	0.55	70	4.32
7	0.63	0.60	80	4.50
8	0.67	0.65	90	4.69
9	0.71	0.70	100	4.90

Note: The maximum forward velocity is the theoretical reference value; TCPCA is the ratio of the square of the forward velocity to the height of the exciter. The forward velocity and the height of the exciter are not taken as experimental factors for easy reference and convenient calculation.

3.3 Simulation

To deeply study the vibration feedback on road elevation changes from the track roller frame system and the inertial impact of the chassis, the simulation needs to be performed to solve the difficult problem that is hard to directly analyze, test, and record in the actual road walking process. In this study, the 3D model built with the software Inventor at the early stage was imported into Recurdyn, a piece of multi-body dynamical analysis software, and the multi-body element combination[29] was used to add kinematic

pairs to each part of the track, create binding force and set flexible winding. The main parameters for the global environment are shown in Table 3.

The initial position is so defined that the lower surface of the track is 50 mm away from the earth's surface. After free falling and stabilization, the driving roller was promoted to rotate through the STEP function. Then, the walking process was simulated at different levels of forward velocity. The simulation time was 20 s and the step length was 1000. The simulation was conducted three times in the test for each group, with a curve chart generated based on the average vertical acceleration of the rear roller. The vertical velocity curve of the chassis at any point was derived as a reference point in the post-processing results. The simulation process is shown in Figure 10. The curve of post-processing results will be analyzed in detail hereinafter by comparing it with the measured results.

Table 3 Global environmental parameter settings for the global environment

Parameters	Value
Road-track-roller train stiffness coefficient	8000
Road-track-roller train damping coefficient	10
Road-track-roller train dynamic friction coefficient	0.2
Rotation stiffness between tracks	10 000
Rotation damping between tracks	1000
Surface type	Quad
Road density/kg m^{-3}	7850
Young's modulus of road/Mpa	2.0×10^5
Road density	0.35
Track density/kg m^{-3}	3100 kg/m^3
Young's modulus of track/Mpa	6
Poisson's ratio of track	0.7

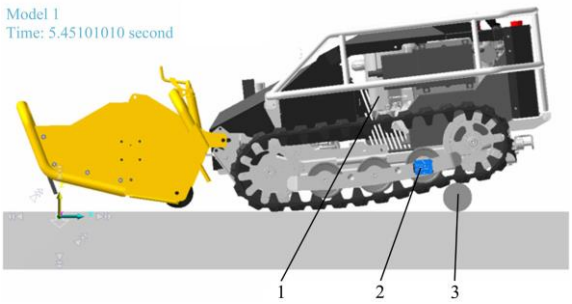

1. Exciter 2. Vibration acceleration sensor 3. Machine model

Figure 10 Screenshot of the virtual simulation process in machine model

3.4 Road surface test

The road surface excitation test was conducted in the Industrialization Demonstration Base, Guangdong Modern Agricultural Equipment Research Institute (National Agricultural Machinery Engineering Technology Research Center South China Branch). A seamless steel tube (thickness: 5 mm; diameter: 20-100 mm) was selected as a cylindrical exciter, which was laid on the tested hard road surface after both ends were splinted firmly. The schematic diagram and test process are shown in Figures 11-13. According to the test design scheme in Table 2, each group underwent the test repeatedly three times, with the data averaged as the final test results.

3.5 Measuring system

The measuring system consists primarily of a sensor, a signal analysis, and processing system, a GPS positioning module, and a mobile monitoring terminal (Figure 12).

The vibration acceleration sensor is the 4400B3 triaxial MEMS portable pallograph (Dytran, USA). It has a built-in battery and SD memory card, and does not require external cable routing or signal acquisition. Also, it can be mounted firmly on the metallic surface of the tested component through strong magnetic adsorption. The technical specifications and performance parameters of the main test equipment are shown in Table 4.

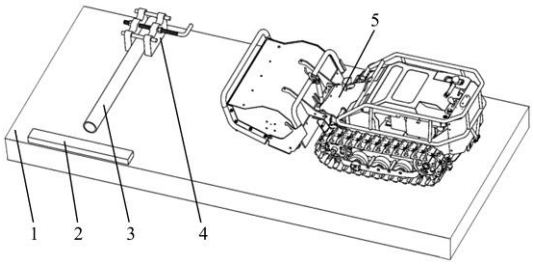

1. Hard road surface 2. Observed end 3. Excitation column tube 4. Exciter clamp 5. Prototype

Figure 11 Schematic diagram of road surface excitation test

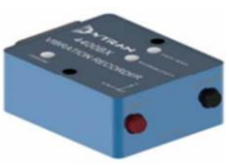

a. Triaxial vibration acceleration sensor

b. Signal analysis and data processing system

c. GPS positioning module

d. Mobile monitoring terminal

Figure 12 Block diagram of the measuring equipment and system

Figure 13 Road surface excitation test process

Table 4 Specifications and parameters of test equipment and software

Name	Main functions and parameters
Triaxial accelerometer (Dytran-4400B3)	Test range: 2-200 g; battery life: 15 h
Information analysis and data processing system (Dytran VibraCorder)	FFT analysis, single and dual integration, oversampling, data superposition, filter processing
GPS positioning module assembly	Velocity accuracy: 0.1 m/s
Mobile monitoring terminal APP	Real-time velocity display, path tracking

4 Results and analysis

4.1 Excitation area positioning

After being exported by VibraCorde, the road test data were extracted. As can be seen from the curve of simulation results, the

vertical acceleration of the target roller fell sharply to a negative value when the track touched the exciter because the entire chassis roller train suffered external impact at this moment; when the track got disengaged from the exciter, the target roller was disengaged instantaneously and then fell to the ground. It suffered impact from the bearing reaction on the ground at the moment it touched the ground. Meanwhile, the vertical acceleration of the target roller fluctuated greatly from the maximum negative value to the maximum positive value. Therefore, it is impossible to locate the time domain of the critical state according to the sudden change rule of the acceleration curve.

4.2 Analysis of vertical vibration acceleration

Nine groups of test data were obtained. The most representative of them, including No. 1, No. 3, No. 5, No. 7, and No. 9 were selected for analysis. Then, according to the simulation results, the time point the moment when the track touched the exciter was approximately intercepted at the adjacent site, as shown in Figures 14a-14e. As can be seen, the thick dash line represents the time domain for entering the critical state.

The curve was analyzed, finding that in the critical state of motion, the effective value of the measured data is slightly greater than that of the simulation results, while the macroscopic change trend is basically the same. This is mainly because the internal vibration of the engine drove the whole machine to generate magnified excitation in the process of field testing. In contrast, the simulation model just worked by adding a power driving command. Therefore, there was a high-frequency vibration error between the measured data and the simulation results.

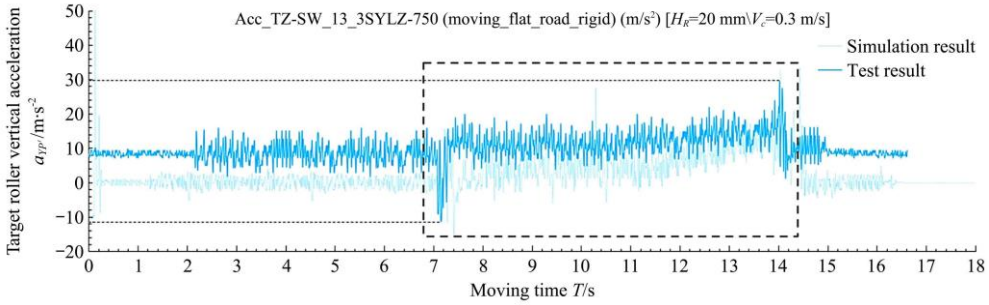

a. Changing curve of vertical acceleration curve of the target roller at a_c=4.5 m/s^2

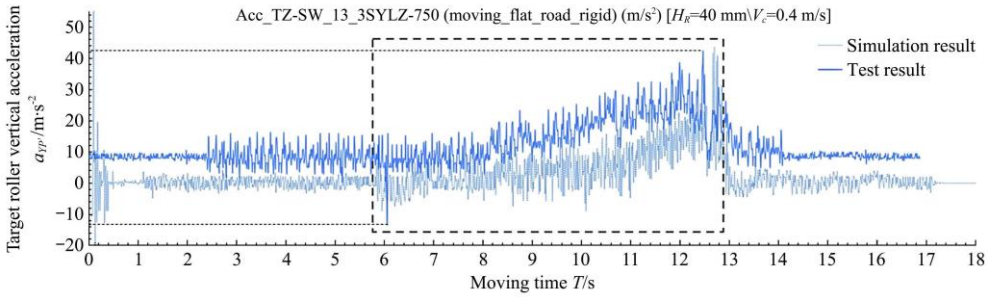

b. Changing curve of vertical acceleration curve of the target roller at a_c=4.0 m/s^2

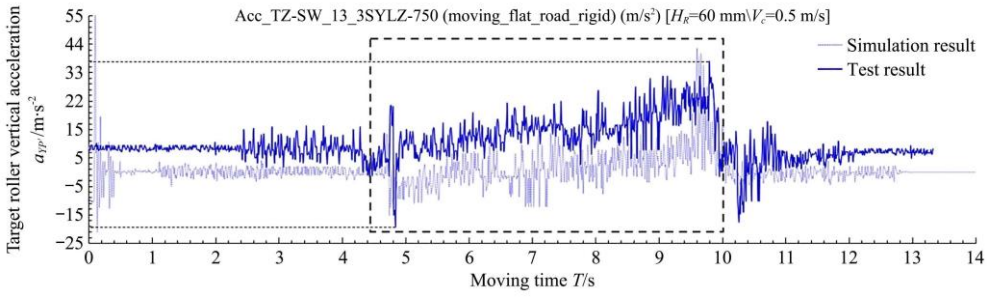

c. Changing curve of vertical acceleration curve of the target roller at a_c=4.16 m s^{-2}

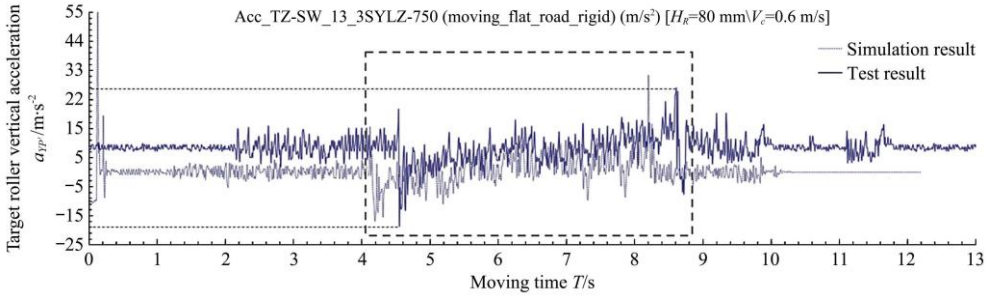

d. Changing curve of vertical acceleration curve of the target roller at a_c=4.5 m/s^2

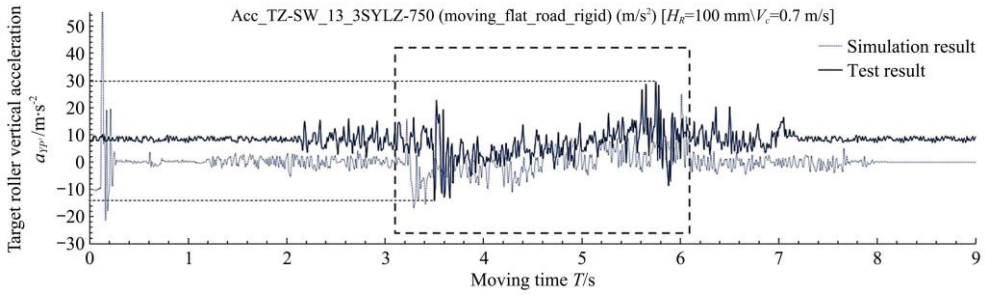

e. Changing curve of vertical acceleration curve of the target roller at a_c=4.9 m s^{-2}

Figure 14 Simulation results and road surface test data

As can be seen from Figures 14b-14e, as the centrifugal acceleration a_c at the point of contact increased gradually, the vertical acceleration $a_{YP'}$ of the target roller changed less and less significantly and became increasingly stable. As shown in Figure 14e, a_c reached its maximum in the No. 9 group, i.e., when a_c= 4.9 m/s^2, the measured change interval of the corresponding $a_{YP'}$ was [−13.8, 28.8]; when the centrifugal acceleration a_c decreased gradually, the vertical acceleration of the target roller increased gradually. Moreover, The smaller the a_c was, the closer the change range was to the exponential growth trend; As shown in Figure 14b, a_c reached its minimum in No.3, i.e., when a_c=4.0 m/s^2, the vertical acceleration of the target roller could reach its maximum at the moment when the front end of the track touched the ground. Besides, the change amplitude increased as the velocity declined, and the measured change interval of the corresponding $a_{YP'}$ was [−13.3, 42.2].

Compared Figure 14a with Figure 14d, it is can be seen that given the same centrifugal acceleration (a_c=4.5 m/s^2), the vertical acceleration $a_{YP'}$ of the target roller did not change significantly, but almost became stable. The measured change intervals of the corresponding $a_{YP'}$ were [−11.1, 29.1] and [−16.6, 28.7], respectively.

According to the above analysis, the macroscopic change trend of virtual test and road surface excitation test results was basically the same as the theoretical model analysis (Figure 6). A grouping test was conducted with a comparison made among different groups, verifying the correctness of the variable analysis, and confirming that TCPCA (the ratio of the square of the forward velocity to the radius of the exciter) has a significant impact on the change in the vertical acceleration of the target roller. The interaction between the forward velocity and the height of the exciter might be mainly manifested in the initial theoretical relationship of TCPCA.

In addition, as shown by the experimental results, the acceleration change range presented in the simulation results was wider than that predicted in the theoretical model, and similarly, the measured acceleration change range was equally wider than that presented in the simulation results. The reason for this phenomenon might be that the track surface was regarded as a smooth rigid body in the theoretical model for mathematical modeling and analysis. Convex-concave patterns were added to the outer surface of the track in the simulation model, and road-contact parameters were set, too, making it possible to discover obvious bumpy vibration in the simulated process of walking calculation. Under the action of external excitation, the center of vibration in the vertical direction was no longer the theoretical zero point. Moreover, because the non-deformed hard road surface always provided a continuous supporting reaction for the track, the vertical acceleration would inevitably rise to a positive value until convergence. Similarly, in the actual road surface excitation test, the transmission actuators inside the prototype, including the engine and hydraulic pump, suffered from complicated high-frequency self-excited vibration, inevitably causing the point of vibrational equilibrium to rise to a positive value, resulting in a difference from the theoretical prediction model.

5 Conclusions

1) A column-type test-to-pass method based on unit excitation was proposed in this study with respect to the research on the walking reliability of a tracked agricultural robot in a complex environment. The theoretical analysis showed that the main factors affecting the vertical acceleration of walking vibration include the square of the track forward velocity and the radius of the exciter. So, a model was built to predict the vibration of the track chassis excited by a sudden change in road elevation. A basis was also established for evaluation.

2) According to the theoretical model and the analysis of the variable relations, track contact point centrifugal acceleration (TCPCA) was taken as a major element, with nine groups of different test schemes designed. Then, a virtual simulation test and road surface excitation test were conducted successively. The test results showed that the change in the vertical vibration acceleration of the target roller was mainly affected by TCPCA. The test results were basically the same as the macroscopic change rule presented in the theoretical model, i.e., as TCPCA increases, the vertical acceleration change range at the target point decreases. On the contrary, the vertical acceleration change range at the target point gradually increases in the positive direction, and the change range increases, thereby verifying the correctness of the research method and theoretical analysis of the excitation behavior.

3) According to the discussion and analysis of the test results, during the walking process of the track chassis, the effective value of the vertical vibration acceleration was also affected by the patterns on the outer surface of the track, road surface excitation, and the vibration of the interior power source of the chassis. Although the non-loaded vibration acceleration of the engine was introduced into the prediction model as a reference and the prediction model was modified in this study, the value range error is greatly affected by the self-excitation of the interior power and track patterns, so the method still cannot be effectively used for actual prediction. In future research, it is necessary to further investigate internal and external coupling excitation, and further improve the accuracy of the model so as to provide a reliable analysis method and design basis for the development of a tracked agricultural robot chassis that can well work in an unstructured environment.

Acknowledgements

This study was financially supported by the Guangdong Provincial Key Project R&D Program (Grant No. 2019B090922001), and the Guangdong Provincial Postdoctoral Research Center Construction Project (Grant No. [2020] No.122). The authors also acknowledge the reviewers for their constructive suggestions on improving this manuscript.

[References]

[1] Li M T, He L, Zhang X, Wu W B. Review of moving reliability analysis methods for agricultural robots in hilly and mountainous areas. International Agricultural Engineering Journal, 2021; 30(1): 1–13. (in Chinese)

[2] Wang W W, Chen L Q, Yang Y, Liu L C. Development and prospect of agricultural machinery chassis technology. Transactions of the CSAM, 2021; 52(8): 1–15. (in Chinese)

[3] Wei K F. Research on steering resistance of tracked vehicle on soft ground based on DEM-MBD simulation. PhD dissertation. Changchun: Jilin University, 2020; 75p. (in Chinese)

[4] Ding Z, Li Y M, Ren L D, Tang Z. Distribution uniformity of soil stress under compaction of tracked undercarriage. Transactions of the CSAE, 2020; 36(9): 52–58. (in Chinese)

[5] Keller T, Arvidsson J. A model for prediction of vertical stress distribution near the soil surface below rubber-tracked undercarriage systems fitted on agricultural vehicles. Soil and Tillage Research, 2016; 155: 116–123.

[6] Chi Y, Zhang R R, Ren J, Li H H, Wang Y. Steering power ratio affected by soil sinkage with differential steering in tracked vehicle. Transactions of the CSAE, 2016; 32(17): 62–68. (in Chinese)

[7] Zhu X G, Gu L. Research on envelope characteristics of the track on ground. Transactions of Beijing Institute of Technology, 2016; 36(1): 48–52. (in Chinese)

[8] Jiang H B, Li X L, Wang G Y. Filtering effect of track on road excitation. Vehicle & Power Technology, 2014; 2: 20–23. (in Chinese)

[9] Mudarisov S, Gainullin I, Gabitov I, Hasanov E, Farhutdinov I. Soil compaction management: reduce soil compaction using a chain-track tractor. Journal of Terramechanics, 2020; 89: 1–12.

[10] Bekker M G. Theory of land locomotion: Mechanics of vehicle mobility. The University of Michigan Press, 1956; pp.199–222.

[11] Bekker M. G. Off the road locomotion. The University of Michigan Press, 1960, 7–94.

[12] Bekker M G. Introduction to terrain-vehicle systems. The University of Michigan Press, 1969; pp.58–62.

[13] Tian F. Body vibration and dynamic response analysis of tracked vehicles. Master dissertation. Shenyang: Shenyang Institute of Technology, 2013; 66p. (in Chinese)

[14] Zhu X G. Coupling dynamic characteristic research for rollers-track-terrain system of high-speed tracked vehicles. PhD dissertation. Beijing: Beijing Institute of Technology, 2015; 146p. (in Chinese)

[15] Yao Y. Research on the trafficability of low-speed tracked vehicle based on track-soil coupling system. PhD dissertation. Changchun: Jilin University, 2016; 113p. (in Chinese)

[16] Nishiyama K, Nakashima H, Shimizu H, Miyasaka J, Ohdoi K. 2D FE-DEM analysis of contact stress and tractive performance of a tire driven on dry sand. Journal of Terramechanics, 2017; 74: 25–33.

[17] Nishiyama K, Nakashima H, Yoshida T, Shimizu H, Miyasaka J, Ohdoi K. FE-DEM with Interchangeable modeling for off-road tire traction analysis. Journal of Terramechanics, 2018; 78: 15–25.

[18] Nakata T, Sogabe Y, Araki T. Vibration property of a rubber track system when traveling over bumps. Engineering in Agriculture Environment & Food, 2010; 3(2): 47–53.

[19] Sundaram J, Varadarajan B, Keppanan M. Dynamic behaviour of a trailing arm suspension unit of a tracked vehicle with flexible and rigid elements. International Journal of Heavy Vehicle Systems, 2017; 24(4): 345. doi: 10.1504/IJHVS.2017.10007645.

[20] Xu L Z, Chai X Y, Gao Z P, Li Y M, Wang Y D. Experimental study on driver seat vibration characteristics of tracked combine harvester. Int J Agric & Biol Eng, 2019; 12(2): 90–97.

[21] ISO 2631-1. Mechanical vibration and shock. Geneva, Switzerland: ISO. 1997.

[22] GB/T 10910. Agricultural wheeled tractor and field operation mechanical driver whole body vibration measurement. Standards Press of China, 2004.

[23] GB/T 13876. Agricultural wheeled tractor driver whole body vibration evaluation index. Standards Press of China, 2007.

[24] Q/GDHK 27-2022. 3CYLZ-750 remote control crawler self-propelled weeder. 2022. (in Chinese)

[25] Kuhner K. Motor vehicle and terrain. VDI1, 1935; pp.153–159.

[26] Zhang K J. Vehicle-terramechanics. National Defense Industry Press, 2001; 350p. (in Chinese)

[27] Xu Z M, Ma K, Wang X G; Yang Z D, Huang Y. Research on vibration evaluation of engine. Journal of Machine Design, 2014; 31(3): 90–94. (in Chinese)

[28] Du Xiumei. Research on robust control of magnetorheological suspension based on all terrain vehicle. PhD dissertation. Chongqing University, 2020; 196p. (in Chinese)

[29] Li M T, He L, Zhang X, Chen H. Research on dynamic modeling method and moving vibration test analysis of flexible track system based on multi body element combination method. Modern Agricultural Equipment, 2021; 42(3): 27–34. (in Chinese)